Scientific Research Publishing

Energy and Power Engineering, 2022, 14, 133-145
https://www.scirp.org/journal/epe
ISSN Online: 1947-3818
ISSN Print: 1949-243X

Impact of the Thicknesses of the p and p$^+$ Regions on the Electrical Parameters of a Bifacial PV Cell

Ramatou Konate[1], Bernard Zouma[1*], Adama Ouedraogo[1,2], Bruno Korgo[1], Martial Zoungrana[1], Sié Kam[1]

[1]Laboratoire d'Energies Thermiques REnouvelables (L.E.T.RE), Département de Physique, Unité de Recherche et de Formation en Sciences Exactes et Appliquées, Université Joseph KI-ZERBO, Ouagadougou, Burkina Faso
[2]Centre Universitaire Polytechnique de Kaya (CUP-Kaya), Kaya, Burkina Faso
Email: *bernard_zouma@ujkz.bf

How to cite this paper: Konate, R., Zouma, B., Ouedraogo, A., Korgo, B., Zoungrana, M. and Kam, S. (2022) Impact of the Thicknesses of the p and p$^+$ Regions on the Electrical Parameters of a Bifacial PV Cell. *Energy and Power Engineering*, **14**, 133-145.
https://doi.org/10.4236/epe.2022.142006

Received: January 14, 2022
Accepted: February 19, 2022
Published: February 22, 2022

Abstract

The present paper is about a contribution to the bifacial PV cell performances improvement. The PV cell efficiency is weak compared to the strong energy demand. In this study, the base thickness impacts and the p$^+$ zone size influence are evaluated on the rear face of the polycrystalline back surface field bifacial silicon PV cell. The photocurrent density and photovoltage behaviors versus thickness of these regions are studied. From a three-dimensional grain of the polycrystalline bifacial PV cell, the magneto-transport and continuity equations of excess minority carriers are solved to find the expression of the density of excess minority carriers and the related electrical parameters, such as the photocurrent density, the photovoltage and the electric power for simultaneous illumination on both sides. The photocurrent density, the photovoltage and electric power versus junction dynamic velocity decrease for different thicknesses of base and the p$^+$ region increases for simultaneous illumination on both sides. It is found that the thickness of the p$^+$ region at 0.1 μm and the base size at 100 μm allow reaching the best bifacial PV cell performances. Consequently, it is imperative to consider the reduction in the thickness of the bifacial PV cell for exhibition of better performance. This reduced the costs and increase production speed while increasing conversion efficiency.

Keywords

Doped p$^+$ Region, Bifacial PV Cell, Photocurrent Density, Photovoltage, Polycrystalline Solar Cell

1. Introduction

Silicon remains the basic material for the design of solar panels on the market. Currently, on the market in Sahelian countries, the most widely used technology is the polycrystalline silicon PV cell because of its best resistance to heat. The PV cell efficiency is weak, around 26% [1]. However, the energy demand is very strong. The PV cell performances improvement is a major preoccupation today. This improvement is obtained by optimizing various parameters [2] [3]. Among these parameters include the semi-conductor doping level, the quality of the material used in the manufacture of PV cells and the different layers of the bifacial PV cell.

Reducing the thickness of the bifacial PV cell results in better efficiency [4] When the thickness is reduced, the rear face recombinations are minimized. Then, for a monofacial cell, parameters such as photocurrent density, electrical power, fill factor, and efficiency increase as the optimum base thickness increases [5]. On the other hand, the photovoltage decreases for a polycrystalline silicon PV cell made up of grains [6], separated from one another by boundaries which themselves also exhibit electrical activity [7]. In addition, generating sources of magnetic field located near photovoltaic installations have negative effect on the performance of PV cells [8]. It is therefore essential to associate these sources in this study to evaluate their influence on the PV cell while its layer size varied.

However, some previous studies carried out in 1D do not allow this granular structure of the grains to be taken into account. In addition, some studies have found an overestimation in 1D models [9], hence the interest of carrying out in 3D study which takes all these aspects into consideration during modeling, particularly through the boundary conditions of grain boundaries.

This work provides in 3D study the influence of the thickness of the overdoped rear region p^+ on the electrical parameters of a polycrystalline back surface field bifacial silicon solar cell. This takes into account not only multispectral illumination but also the contribution of an external magnetic field. This investigation will lead us to identify the best thickness range of p^+ doped region which can help to optimize the contribution of the illumination by the rear side.

In this paper, the assumptions and resolutions of the equations will be given in the section titled methods and theories. The impact of the base thickness and p^+ region on the photocurrent density and photovoltage of the bifacial PV cell for simultaneous illumination on both sides will be presented in the section titled results and discussions. Conclusion will be drawn at the end of our work.

2. Methods and Theories

2.1. Assumptions and Basics Equations

The model in this study is a three-dimensional (3D) grain extracted from a bifacial Polycrystalline silicon solar cell, which possesses mainly three regions: The emitter, the base and overdoped p^+ region with an active albedo surface. **Figure 1** provides the gain features.

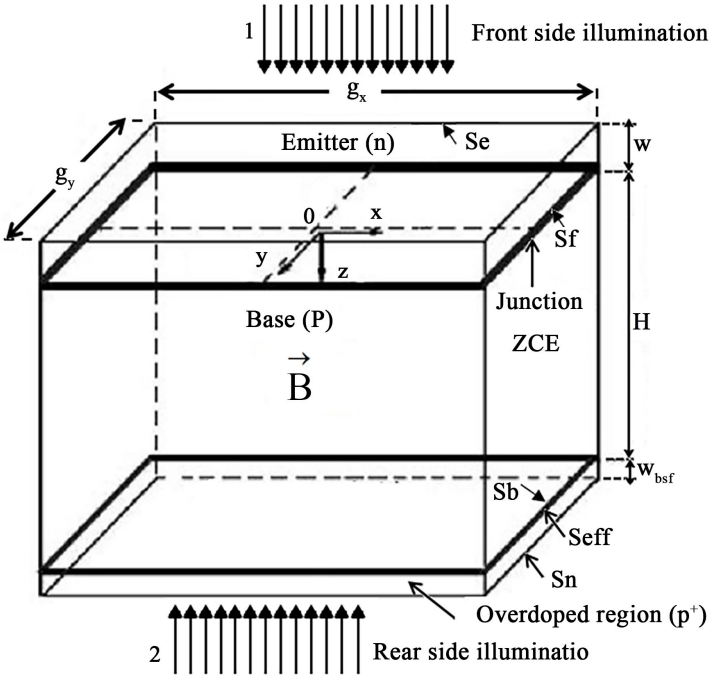

Figure 1. 3D model of the grain of bifacial silicon PV cell [10].

On This figure, in the emitter, we have $-W \le z \le 0$, while in the base $0 \le z \le H$ and in the p⁺ region $H \le z \le H + Wbsf$.

Different hypotheses are necessary in order to facilitate establishment and resolution of equations:

1) The generation of minority excess charge carriers takes place along the direction (OZ) which is perpendicular to the junction also called space charge region (SCR) where there is an electric field [11]. W, H and Wbsf are respectively the thicknesses of the emitter, base and the overdoped region, g_x and g_y are the sizes of grain along x and y axis, they determine the flat surface receiving the light.

2) The joints of the grain are located at $x = \pm\frac{g_x}{2}$ and $y = \pm\frac{g_y}{2}$ for the origin of the coordinate system is in the center of the flat surface [11].

3) The emitter, base and p⁺ regions are quasi-neutral at the thermodynamic equilibrium. The internal electric field is neglected. The intensity of the magnetic field is constant and directed along (OY) axis, $\boldsymbol{B} = B\boldsymbol{j}$.

4) The boarder's effects induced by the magnetic field are neglected, for as one should in principle have charge spreading on the lateral sides of the grain because of the Hall Effect due to the presence of the magnetic field. The flat surface of the grain is considered to be square, which means $g_x = g_y$.

5) The shading effects of the collector grids on the two sides of the solar cell are taken into account; but we only take into account the reflection on the silicon material, the external sides of the solar cell being covered with an anti-reflecting layer. The effect of temperature on the performance of the solar cell

is not taken into account.

The 3D continuity equations steady state in the base and p^+ region obtained from the magnetotransport equations in these regions are given by [12]:

✓ In the base

$$\frac{\partial^2 \delta_n}{\partial x^2} + \left(1 + (\mu B)^2\right) \frac{\partial^2 \delta_n}{\partial y^2} + \frac{\partial^2 \delta_n}{\partial z^2} - \frac{\delta_n}{\tau_n D_n^*} + \frac{G_\sigma}{D_n^*} = 0 \tag{1}$$

✓ In the p^+ region

$$\frac{\partial^2 \delta_{n^+}}{\partial x^2} + \left(1 + (\mu B)^2\right) \frac{\partial^2 \delta_{n^+}}{\partial y^2} + \frac{\partial^2 \delta_{n^+}}{\partial z^2} - \frac{\partial_{n^+}}{L_{n^+}^*} + \frac{G}{D_{n^+}^*} = 0 \tag{2}$$

Generation rate $G_o(z)$ is given by [13]:

Simultaneous illumination on both sides ($\sigma = 1,2$)

$$G_{12}(z) = n \sum_{m=1}^{3} a_m \left[e^{-b_m[W+z]} + e^{-b_m[H+Wbsf-z]} \right] \tag{3}$$

The coefficients are obtained from tabulated values of solar irradiance. The coefficient n is called "number of suns".

2.2. Exess Minority Charge Carriers Density

The electrons are the excess minority charge carriers in the base and in the p^+ region. However, minority charge carriers are the holes.

The laws of evolution of the diffusion coefficient and lifetime of the electrons in these two regions as a function of the doping rate are also given in this subsection.

The expressions of diffusion coefficient and lifetime in the base region are given by Liou *et al.* [14]:

$$D_n(Nb) = 1350Vt \frac{1}{\sqrt{1 + \frac{81Nb}{Nb + 3.2 \times 10^{18}}}} \tag{4}$$

$$\tau_n(Nb) = \frac{1}{1 + \frac{Nb}{5 \times 10^{16}}} \tag{5}$$

The doping level of the base is represented by Nb and VT is the thermal voltage.

In the overdoped region p^+ the diffusion coefficient and the lifetime are given by Swirhun *et al.* [15]:

$$D_n' bsf = Vt \left[232 + \frac{1180}{1 + \left(\frac{Nbsf}{8 \times 10^{16}} \right)^{0.9}} \right] \tag{6}$$

$$\tau_n' bsf = \frac{1}{3.45 \times 10^{-12} Nbsf + 0.95 \times 10^{-31} Nbsf^2} \tag{7}$$

Equation (1) is a second-order differential equation with constant coefficient

and whose solution is given by (8) below [12]:

$$\delta_{n\sigma}(x,y,z)=\sum_{j}\sum_{k}Z_{n\sigma jk}(z)\cos(c_j x)\cos\left(\frac{c_k}{\theta}y\right) \tag{8}$$

where $\theta^2=1+(\mu B)^2$

For simultaneous illumination on both sides, Z is given by the following relationship:

$$\begin{aligned}Z_{n12\,jk}(z)=&A_{n1\,jk}\cosh\left(\frac{z}{L^*_{njk}}\right)+B_{n1\,jk}\sinh\left(\frac{z}{L^*_{njk}}\right)+A_{n2\,jk}\cosh\left(\frac{z}{L^*_{njk}}\right)\\&+B_{n2\,jk}\sinh\left(\frac{z}{L^*_{njk}}\right)-\sum_{m=1}^{3}T_{njk}\left[\mathrm{e}^{-b_m[W+z]}+\mathrm{e}^{-b_m[H+Wbsf-z]}\right]\end{aligned} \tag{9}$$

The constants $A_{n\sigma\,jk}$ and $B_{n\sigma\,jk}$ are determined from boundaries conditions taken at two different positions which are: the junction ($z=0$) and the rear side ($z=H$).

At the junction

$$\left.\frac{\partial\delta_{n\sigma}(x,y,z)}{\partial z}\right|_{z=0}=S_{fn\sigma}\frac{\delta_{n\sigma}(x,y,0)}{D^*_n} \tag{10}$$

At the interface base-p^+ region

$$\left.\frac{\partial\delta_{n\sigma}(x,y,z)}{\partial z}\right|_{z=H}=-Sb\frac{\delta_{n\sigma}(x,y,H)}{D^*_n} \tag{11}$$

Electron density in the base is obtained by replacing Z, in Equation (8).

The electron density in the p^+ region is evaluated through Equation (2) as well.

For simultaneous illumination on both sides, we have the following relationships,

$$\begin{aligned}Z_{n^+12\,jk}(z)=&A_{n^+1\,jk}\cosh\left(\frac{z}{L_{jk}}\right)+B_{n^+1\,jk}\sinh\left(\frac{z}{L_{jk}}\right)+A_{n^+2\,jk}\cosh\left(\frac{z}{L_{jk}}\right)\\&+B_{n^+2\,jk}\sinh\left(\frac{z}{L_{jk}}\right)-\sum_{m=1}^{3}T_{njk}\left[\mathrm{e}^{-b_m[W+z]}+\mathrm{e}^{-b_m[H+Wbsf-z]}\right]\end{aligned} \tag{12}$$

The real constants A and B are found by the boundaries conditions in p^+ region are:

At the interface base-p^+ region

$$\left.\frac{\partial\delta_{n^+\sigma}(x,y,z)}{\partial z}\right|_{z=H}=Seff\frac{\delta_{n^+\sigma}(x,y,H)}{D^*_{n^+}} \tag{13}$$

At the rear side

$$\left.\frac{\partial\delta_{n^+\sigma}(x,y,z)}{\partial z}\right|_{z=H+W_{bsf}}=-S_n\frac{\delta_{n^+\sigma}(x,y,H+W_{bsf})}{D^*_{n^+}} \tag{14}$$

Once Z have been found, it is replaced in Equation (8) to obtain the density

carrier charges in p^+ region.

3. Photocurrent Density and Photovoltage

For evaluation of photocurrent density and photovoltage, we will consider a square surface grain of bifacial solar cell of size 0.01 cm ($g_x = g_y = 0.01$ cm) with the same recombination velocity in the joints for the base and the emitter (Sg = 100 cm·s^{-1}). We consider the impact of the magnetic field which is a factor which degrades the fundamental parameters of the PV cell [16]. The doping rate of the base is set at 10^{16} cm^{-3}, the p^+ region at 10^{19} cm^{-3}, and that of the emitter at 10^{18} cm^{-3} [17].

3.1. Photocurrent Density

The electrons and holes photocurrent density is a function of the gradients of excess minority charge carriers. For simultaneous illumination on both sides, the density of the photocurrent in the base is given by [18]:

$$J_{n12}\left(Sf, B, Nb\right) = eD_n \sum_{j=0}^{\infty}\sum_{k=0}^{\infty} S_{njk}\left[\frac{B_{n12\,jk}}{L^*_{njk}} + \sum_{m=1}^{3} b_m T_{njk}\left[\mathrm{e}^{-b_m W} - \mathrm{e}^{-b_m[H+Wbsf]}\right]\right] \quad (15)$$

For simultaneous illumination on both sides, the density of the photocurrent y is presented as follows in the overdoped p^+ region:

$$J_{n^+12}\left(Sf, B, Nbsf, n\right) = eD^*_{n^+}\sum_{j=0}^{\infty}\sum_{k=0}^{\infty} S_{n^+jk}\left[\frac{A_{n^+12\,jk} + B_{n^+12\,jk}}{L_{n^+jk}} + \sum_{m=1}^{3} b_m T_{n^+jk}\left[\mathrm{e}^{-b_m[W+H]} - \mathrm{e}^{-b_m\left[W_{bsf}\right]}\right]\right] \quad (16)$$

3.2. Photovoltage

The voltage which exists in the terminals of the PV cell under illumination is found using the Boltzmann relation [19].

For simultaneous illumination on both sides, the photovoltage in the base is given by the relation below:

$$V_{phn12}\left(Sf, B, Nb\right) = V_T \ln\left(1 + \frac{1}{n_0} * \sum_{j=0}^{\infty}\sum_{k=0}^{\infty} S_{n'jk}\left(A_{n12\,jk} - \sum_{m=1}^{3} T_{njk}\left[\mathrm{e}^{-b_m W} + \mathrm{e}^{-b_m(H+Wbsf)}\right]\right)\right) \quad (17)$$

For simultaneous illumination on both sides, the photovoltage in the overdoped region p^+ is evaluated by the relation (18).

$$V_{phn^+12}\left(Sf, B, Nbsf\right) = V_T \ln\left(1 + \frac{1}{n_0} * \sum_{j=0}^{\infty}\sum_{k=0}^{\infty}\left(Z_{n^+12\,jk}\left(H\right)\right) S_{n^{+\prime}jk}\right) \quad (18)$$

The determination of the intrinsic parameters such as diffusion coefficient, lifetime and the densities of minority charge carriers in addition to the assessment of the extrinsic parameters such as photovoltage and photocurrent density was carried out in this section. In the next section, the results and discussions about the thickness influence on the extrinsic parameters will be given.

4. Results and Discussions

In the present section, the influence of both base thickness and p^+ region thickness on photocurrent, photovoltage and electric power is presented. It is first shown the impact of the base thickness on the bifacial PV cell photocurrent, photovoltage and electrical power. That will allow us to find a better base thickness which u will be used to simulate the influence of the p^+ region thickness variation on the density photocurrent, the photovoltage and the electrical power.

4.1. Impact of the Thickness of the Base on the Photocurrent Density

Figure 2 represents the photocurrent density versus recombination velocity at the junction for different base thicknesses under simultaneous illumination on both sides.

It appears on this figure that the increase of the base thickness leads to the decrease in the photocurrent density from 100 µm to 300 µm in Short-circuit (high junction dynamic velocity) reveled an increase, in open circuit (low junction dynamic velocity) and in intermediate operating mode (between open circuit and short-circuit). Indeed, the increase in the base region size leads to a widening of the active area for the collection of excess minority carriers; this explains the improvement in intermediate mode. However, as the size of the base region increases, the distance to be traveled by the charge carriers exceeds the diffusion length and this leads to the drop of short-circuit photocurrent beyond 200 µm.

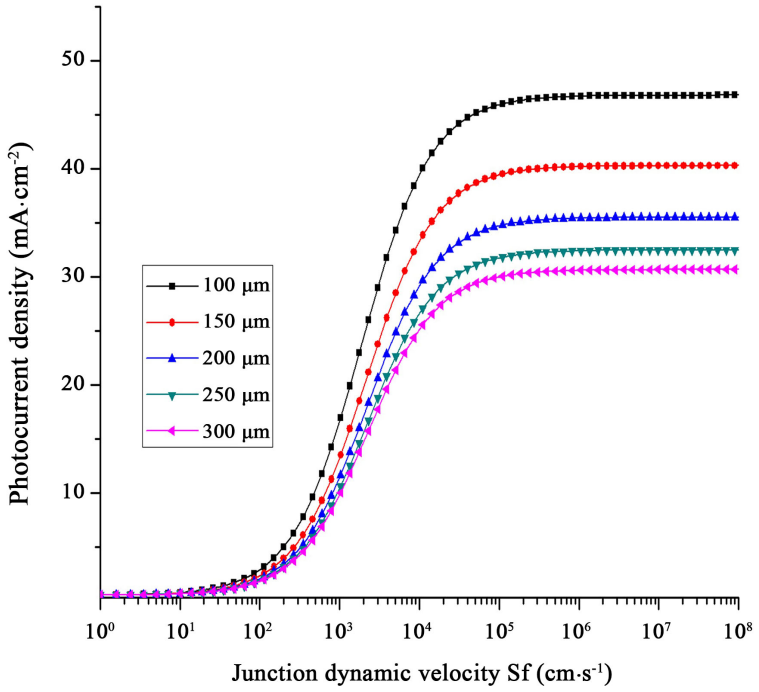

Figure 2. Photocurrent density versus junction dynamic velocity for different thicknesses of the base ($Nb = 10^{16}$ cm^{-3}, $Ne = 10^{18}$ cm^{-3}, $Wbsf = 0.1$ µm, $W = 0.1$ µm, $B = 5 \times 10^{-5}$ T).

4.2. Impact of the Thickness of the Base on the Photovoltage

The figure below shows the photovoltage versus junction dynamic velocity for different base thicknesses under simultaneous illumination on both sides.

As shown in Figure 3, the photovoltage decreases as the thickness of the base region increases. This decrease is clearly observed in open circuit, in intermediate operating mode and short-circuit. In fact, when the thickness of the base region increases, the carriers charge quantity stored at the junction decreases and this situation leads to the decrease in open circuit photovoltage.

4.3. Impact of the Thickness of the Base on the Electric Power

Figure 4 provides the electric power versus the junction dynamic velocity at the junction for different thicknesses of the base region under simultaneous illumination on both sides.

The curves in Figure 4 show that the electric powers are zero in open circuit, then the curves increase up to reach a maximum value before decreasing until canceled in short-circuit. In addition, the electric power decreases when the thickness of the base region increases in open circuit, in intermediate operating mode and, in short-circuit. This is due to the decrease in the number of photons penetrating the base when the thickness of this region increases. So the reduction of the thickness of the base region improves the electrical parameters of the base, and the optimum thickness is at 100 μm. Subsequently, we will set the thickness of the base at 100 μm in order to determine the influence of the over-doped region p^+.

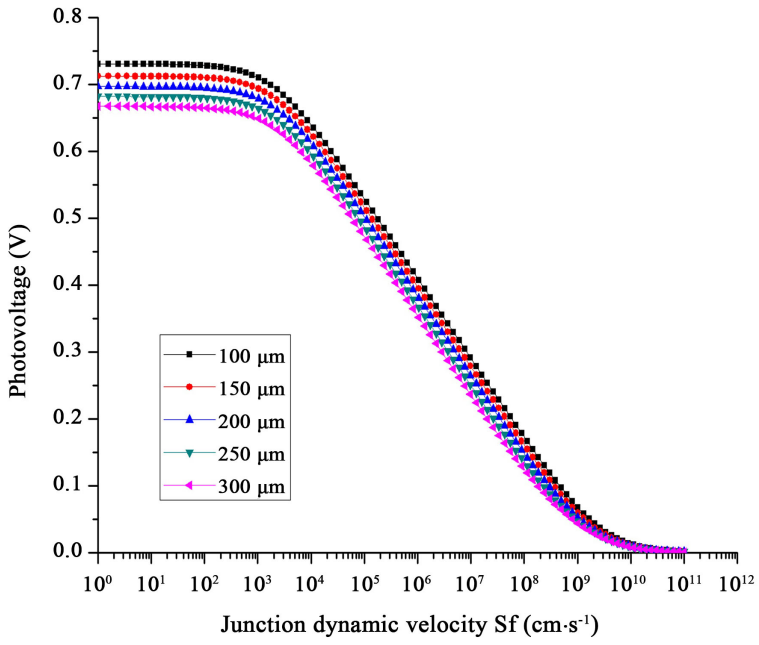

Figure 3. Photovoltage versus junction dynamic velocity for different thicknesses of the base ($Nb = 10^{16}$ cm^{-3}, $Ne = 10^{18}$ cm^{-3}, $Wbsf = 0.1$ μm, $W = 0.1$ μm, $B = 5 \times 10^{-5}$ T).

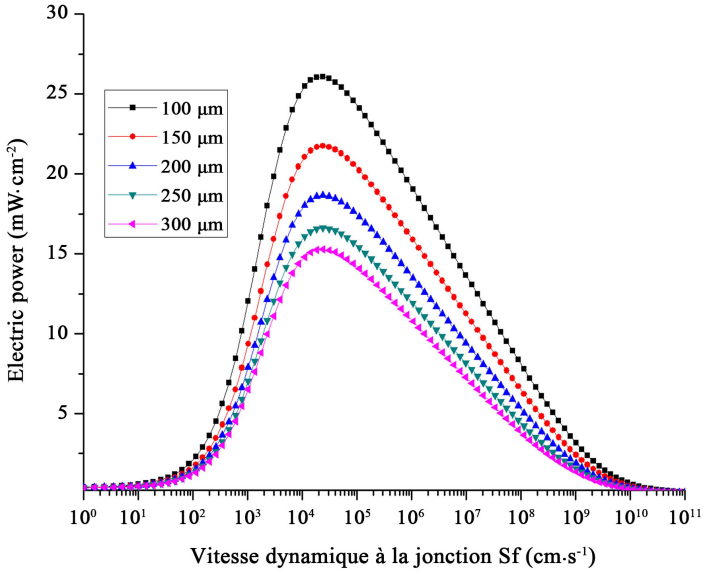

Figure 4. Electric power versus junction dynamic velocity for different thicknesses of the base region ($Nb = 10^{16}$ cm^{-3}, $Ne = 10^{18}$ cm^{-3}, $Wbsf =$ 0.1 µm, $W = 0.1$ µm, $B = 5 \times 10^{-5}$ T).

4.4. Influence of the Thickness of p$^+$ Region on the Photocurrent Density

Figure 5 represents the photocurrent density as the function of the junction dynamic velocity for different thicknesses of the p$^+$ region under simultaneous illumination on both sides.

It appears in the curves of Figure 5 that the short-circuit photocurrent is strongly affected by the thickness of the p$^+$ region increase. Indeed, by moving from 0.1 µm to 10 µm, it is noted a decrease in the short-circuit photocurrent. The thicker the p$^+$ region is, the fewer electrons cross the p-n junction to participate in the external current. This observation was notified in the emitter [10]. Also, it should be noted a weak generation of electrons in the p$^+$ region. The efficiency of the bifacial solar cell necessarily depends on a judicious choice of the thickness of the p$^+$ region. The decrease in the thickness of the rear p$^+$ region also leads to an improvement in the photocurrent. This phenomenon is the consequence of the back surface field which sends back the minority charge carriers in order to prevent them from recombining on the rear side of the cell and ensure a better collection of carriers charge.

4.5. Influence of the Thickness of p$^+$ Region on the Photovoltage

Figure 6 gives the photovoltage versus junction dynamic velocity for different thicknesses of the p$^+$ region.

The curve of photovoltage as a function of junction dynamic velocity decrease weakly when the thickness of the p$^+$ region increases from 0.1 µm to 10 µm. In open circuit, the carriers charge quantity decreases when the thickness of the p$^+$ region increases. When the thickness of the p$^+$ region is large, the path of the

carriers' charge is lengthened and they will be exposed to the phenomenon of recombination, since this region is an absorption region. In short-circuit there are almost no charge carriers at the junction, so no sensitivity of the photovoltage.

4.6. Impact of the Thickness of p^+ Region on the Electric Power

Figure 7 represents the electric power versus junction dynamic velocity for different thicknesses of the p^+ region.

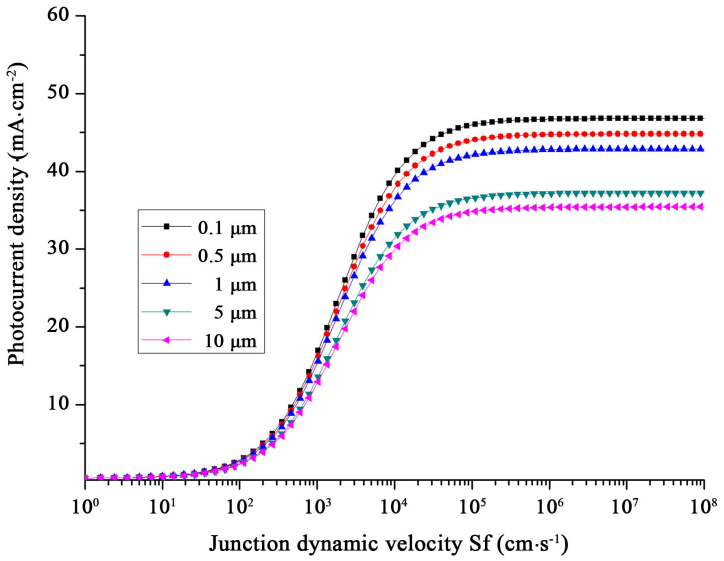

Figure 5. Photocurrent density versus junction dynamic velocity for different thicknesses of the p^+ region ($Nb = 10^{16}$ cm^{-3}, $Ne = 10^{18}$ cm^{-3}, $H = 100$ µm, $W = 0.1$ µm, $B = 5 \times 10^{-5}$ T).

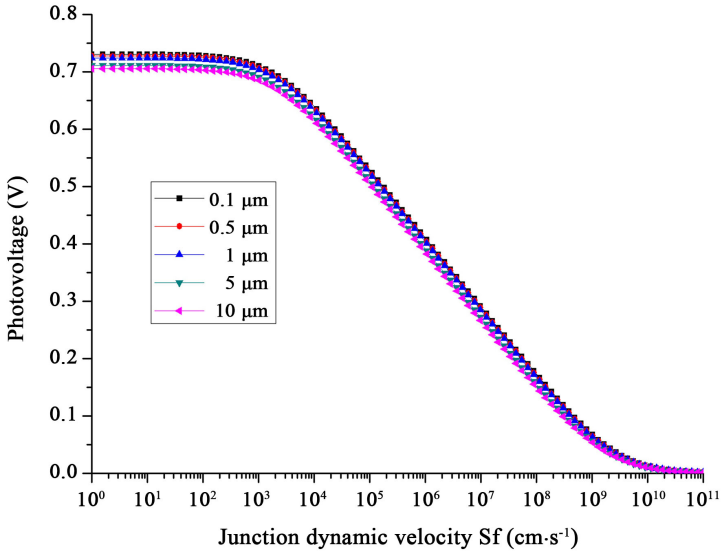

Figure 6. Photovoltage versus junction dynamic velocity for different thicknesses of the p^+ region ($Nb = 10^{16}$ cm^{-3}, $Ne = 10^{18}$ cm^{-3}, $H = 100$ µm, $W = 0.1$ µm, $B = 5 \times 10^{-5}$ T).

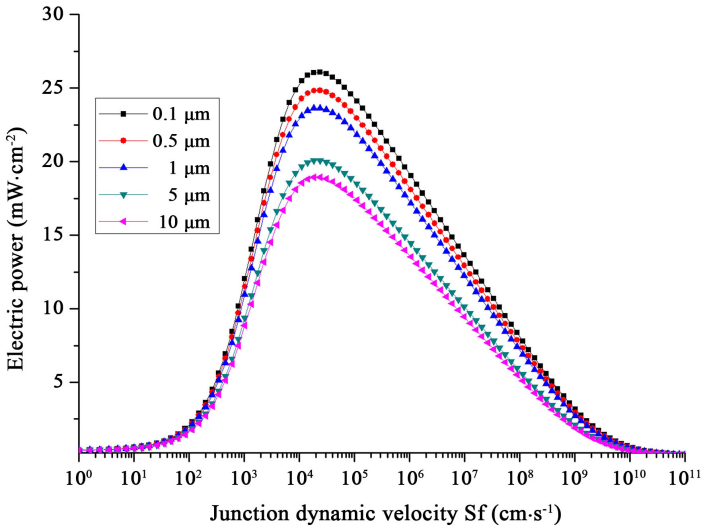

Figure 7. Electric power versus junction dynamic velocity for different thicknesses of the p^+ region ($Nb = 10^{16}$ cm^{-3}, $Ne = 10^{18}$ cm^{-3}, $H = 100$ µm, $W = 0.1$ µm, $B = 5 \times 10^{-5}$ T).

The curves in Figure 7 show that the electric power in open circuit in intermediate operating mode and in short circuit, the electrical power decreases when the thickness of the p^+ zone increases from 0.1 µm 10 µm. Therefore, the thin p^+ region exhibits an improvement in maximum power; consequently, the conversion efficiency is better for the small thickness of the p^+ region.

5. Conclusion

By numerical simulation, the impact of the thickness of the base and the p^+ region has been studied on the density of photocurrent, the photovoltage and the electric power of the polycrystalline bifacial silicon solar cell; those parameters decrease with the increases in the thickness of the base and the p^+ region. The results obtained show that the thickness of the p^+ region at 0.1 µm and that of the base at 100 µm allow reaching the best bifacial cell performance. It is therefore imperative to consider the reduction in the thickness of the bifacial PV cell for exhibition of better performance. Hence, both region thickness reductions can allow the fabrication of low-cost PV cells and PV modules. That can contribute to developing countries' accessibility to energy and a reduction of global climate change.

Acknowledgements

The authors are thankful to International Science Program (ISP) which is supporting our research group.

Conflicts of Interest

The authors declare no conflicts of interest regarding the publication of this paper.

References

[1] Chander, S., Purohit, A., Sharma, A., Nehra, S.P. and Dhaka, M. S. (2015) Impact of Temperature on Performance of Series and Parallel Connected Mono-Crystalline Silicon Solar Cells. *Energy Reports*, **1**, 175-180. https://doi.org/10.1016/j.egyr.2015.09.001

[2] Zoungrana, S.M., Zerbo, I., Soro, B. and Joseph, D. (2017) 3-D Modeling of Grains Sizes Effects on Polycrystalline Silicon Solar Cell under Intense Light Illumination. *SYLWAN English Edition*, **161**, 2-13.

[3] Moharram, K.A. (2013) Enhancing the Performance of Photovoltaic Panels by Water Cooling. *Ain Shams Engineering Journal*, **4**, 869-877. https://doi.org/10.1016/j.asej.2013.03.005

[4] Wolf, M. and Ralph, E.L. (1965) Effect of Thickness on Short-Circuit Current of Silicon Solar Cells. *IEEE Transactions on Electron Devices*, **12**, 470-474. https://doi.org/10.1109/T-ED.1965.15528

[5] Sow, O., Ba, M., El Moujtaba, M., Traore, Y., Sow, E., Sarr, C., Diop, M. and Sissoko, G. (2020) Electrical Parameters Determination from Base Thickness Optimization in a Silicon Solar Cell under Influence of the Irradiation Energy Flow of Charged Particles. *Energy and Power Engineering*, **12** 1-15. https://doi.org/10.4236/epe.2020.121001

[6] Dione, M.M., Thiame, M., Bako, Z.N., Samoura, A., Barro, F.I. and Sissoko, G. (2009) Etude en regime statique d'une photopile au silicium a jonction verticale parallele sous eclairement monochromatique. *Journal des Sciences*, **9**, 43-50.

[7] Rocher, A. (1987) Origine structurale et chimique de l'activité électrique des joints de grains dans le silicium. *Physical Review Applied*, **22**, 591-595. https://doi.org/10.1051/rphysap:01987002207059100

[8] Ouedraogo, A., De Dieu, V., Barandja, B., Zerbo, I., Zoungrana, M. and Ouagadougou, B.F. (2017) A Theoretical Study of Radio Wave Attenuation through a Polycrystalline Silicon Solar Cell. *Turkish Journal of Physics*, **41**, 314-325.

[9] Sam, R., Zouma, B., Zougmoré, F., Koalaga, Z., Zoungrana, M. and Zerbo, I. (2012) 3D Determination of the Minority Carrier Lifetime and the p-n Junction Recombination Velocity of a Polycrystalline Silicon Solar. *IOP Conference Series*: *Materials Science and Engineering*, **29**, Article ID: 012018. https://doi.org/10.1088/1757-899X/29/1/012018

[10] Zouma, B., Maiga, A. S., Dieng, M., Zougmore, F. and Sissoko, G. (2009) 3d Approach of Spectral Response for a Bifacial Silicon Solar Cell under a Constant Magnetic Field. *Global Journal of Pure and Applied Sciences*, **15**, 117-124. https://doi.org/10.4314/gjpas.v15i1.44908

[11] Dugas, J., Oualid, J., Dugas, J., Oualid, J. and De Physique, R. (1987) 3D-Modelling of Polycrystalline Silicon Solar Cells. *Physical Review Applied*, **22**, 677-685. https://doi.org/10.1051/rphysap:01987002207067700

[12] Dugas, J. (1994) 3D Modelling of a Reverse Cell Made with Improved Multicrystalline Silicon Wafers. *Solar Energy Materials and Solar Cells*, **32**, 71-88. https://doi.org/10.1016/0927-0248(94)90257-7

[13] Ngom, M.I., Zouma, B., Zoungrana, M., Thiame, M., Bako, Z.N., Camara, A.G. and Sissoko, G. (2012) Theoretical Study of a Parallel Vertical Multi-Junction Silicon Cell under Multispectral Illumi-Nation: Influence of External Magnetic Field on the Electrical Parameters. *International Journal of Advanced Technology & Engineering Research*, **2**, 101-109.

[14] Liou, J.J. and Wong, W.W. (1992) Comparison and Optimization of the Perfor-

mance of Si and GaAs Solar Cells. *Solar Energy Materials and Solar Cells*, **28**, 9-28. https://doi.org/10.1016/0927-0248(92)90104-W

[15] Swirhun, S.E., Kwark, Y.H. and Swanson, R.M. (1986) Measurement of Electron Lifetime, Electron Mobility and Band-Gap Narrowing in Heavily Doped P-Type Silicon. 1986 *International Electron Devices Meeting*, Los Angeles, 7-10 December 1986, 24-27. https://doi.org/10.1109/IEDM.1986.191101

[16] Zerbo, I., Zoungrana, M., Sourabié, I., Ouedraogo, A. and Zouma, B. (2016) External Magnetic Field Effect on Bifacial Silicon Solar Cell's Electrical Parameters. *Energy and Power Engineering*, **8**, 146-151. https://doi.org/10.4236/epe.2016.83013

[17] Barro, F.I., Sané, M. and Zouma, B. (2015) Theoretical Investigation of Base Doping and Illumination Level Effects on a Bifacial Silicon Solar Cell. *British Journal of Applied Science & Technology*, **7**, 610-618.

[18] Zoungrana, M., Zerbo, I., Ouédraogo, F., Zouma, B. and Zougmoré, F. (2012) 3D Modelling of Magnetic Field and Light Concentration Effects on a Bifacial Silicon Solar Cell Illuminated by Its Rear Side. *IOP Conference Series*: *Materials Science and Engineering*, **29**, Article ID: 012020. https://doi.org/10.1088/1757-899X/29/1/012020

[19] Samb, M.L., *et al.* (2010) Etude en modelisation a 3-D d'une photopile au silicium en regime statique placee dans un champ magnetique et sous eclairement multispectral : determination des parametres electriques Plusieurs techniques de caractérisation du matériau silicium. *Journal des Sciences*, **10**, 23-38. http://www.cadjds.org